

# Cu<sup>I</sup> Thiolate Reactivity with Dioxygen: The Formation of Cu<sup>II</sup> Sulfinate and Cu<sup>II</sup> Sulfonate Species via a Cu<sup>II</sup> Thiolate Intermediate

Erica C.M. Ording-Wenker,<sup>†</sup> Maxime A. Siegler,<sup>‡</sup> Martin Lutz,<sup>§</sup> and Elisabeth Bouwman<sup>\*,†</sup>

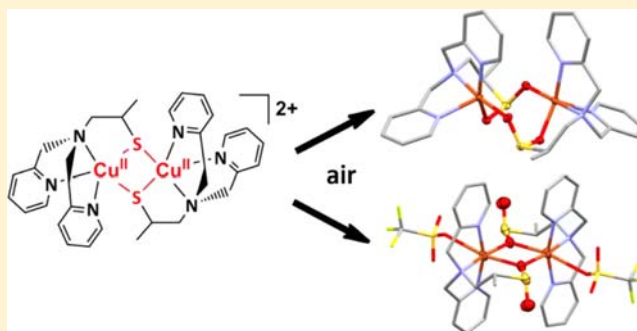
<sup>†</sup>Leiden Institute of Chemistry, Gorlaeus Laboratories, Leiden University, P.O. Box 9502, 2300 RA Leiden, The Netherlands

<sup>‡</sup>Department of Chemistry, Johns Hopkins University, Baltimore, Maryland 21218, United States

<sup>§</sup>Bijvoet Centre for Biomolecular Research, Utrecht University, Padualaan 8, 3584 CH Utrecht, The Netherlands

## Supporting Information

**ABSTRACT:** Cu<sup>I</sup>(Py<sub>2</sub>NS) (**1**) is formed by addition of Cu<sup>I</sup> to a solution of the pyridyl-thiol ligand *N*-(2-mercaptopropyl)-*N,N*-bis(2-pyridylmethyl)amine (Py<sub>2</sub>NSH). Oxidation of complex **1** by air leads to the formation of Cu<sup>II</sup> sulfinate and Cu<sup>II</sup> sulfonate complexes, providing a model for the oxidative degeneration of copper–sulfur enzymes. Crystal structures were obtained for two Cu<sup>II</sup> sulfinate complexes, [Cu<sup>II</sup><sub>2</sub>(Py<sub>2</sub>NSO<sub>2</sub>)<sub>2</sub>](BF<sub>4</sub>)<sub>2</sub>·2(CH<sub>3</sub>)<sub>2</sub>CO (**4a**) and [Cu<sup>II</sup><sub>2</sub>(Py<sub>2</sub>NSO<sub>2</sub>)<sub>2</sub>(OTf)<sub>2</sub>] (**4b**), which were further characterized by UV–vis and EPR spectroscopy and cyclic voltammetry. Furthermore, two Cu<sup>II</sup> sulfonate complexes with the proposed formulas Cu<sup>II</sup><sub>2</sub>(Py<sub>2</sub>NSO<sub>3</sub>)<sub>2</sub>(BF<sub>4</sub>)<sub>2</sub> (**5a**) and Cu<sup>II</sup><sub>2</sub>(Py<sub>2</sub>NSO<sub>3</sub>)<sub>2</sub>(OTf)<sub>2</sub> (**5b**) have been isolated and characterized. Monitoring the oxidation of **1** by UV–vis indicates that the oxidation proceeds via a dinuclear Cu<sup>II</sup> μ-thiolate complex (**3**); as an intermediate an octanuclear mixed-valent Cu<sup>I</sup><sub>4</sub>Cu<sup>II</sup><sub>4</sub> cluster with formula [Cu<sup>I</sup><sub>4</sub>Cu<sup>II</sup><sub>4</sub>(Py<sub>2</sub>NS)<sub>4</sub>(μ-OH)<sub>2</sub>(CH<sub>3</sub>CN)<sub>6</sub>](ClO<sub>4</sub>)<sub>6</sub>·2CH<sub>3</sub>CN (**2**) was isolated and characterized by X-ray single crystal structure determination.



## INTRODUCTION

Copper plays an essential role in many biological processes. Its ability to cycle between the Cu<sup>II</sup> and Cu<sup>I</sup> oxidation states makes it a suitable active site in a wide range of enzymes. A large group of these copper-containing proteins have a coordinating sulfur atom within their active site, which can mediate oxidation and reduction reactions.<sup>1</sup> Examples of this type of enzyme are dopamine β-mono-oxygenase (DβM)<sup>2</sup> and peptidylglycine α-hydroxylating mono-oxygenase (PHM).<sup>3–5</sup> These enzymes have two copper centers in their active site, denoted as Cu<sub>M</sub> and Cu<sub>H</sub>, which catalyze the formation of hydroxylated products.<sup>6</sup> The Cu<sub>M</sub> site, which activates the dioxygen molecule, has a long axial Cu–S methionine bond. Another group of proteins that are involved in electron transfer comprise the so-called blue copper proteins.<sup>7,8</sup> These enzymes contain an active site in which the copper center is strongly coordinated to a cysteine thiolate donor. The Cu–S bond has a highly “covalent” character, which gives rise to an intense blue color due to a ligand to metal charge transfer (LMCT) of S<sup>−</sup> to Cu<sup>II</sup>.<sup>9</sup> The dinuclear Cu<sub>A</sub> site that is found in cytochrome c oxidase (CcO)<sup>10–12</sup> and N<sub>2</sub>O reductase<sup>13</sup> also functions as an electron-transfer catalyst. The Cu<sub>A</sub> active site contains two copper centers bridged by two cysteine ligands with a delocalized mixed valence resting state of Cu<sup>I.5</sup>Cu<sup>1.5</sup>. These are a few examples of the copper–sulfur enzymes that are known, and many of these copper proteins are involved in O<sub>2</sub> activation reactions. It is therefore important to know how

oxidation-sensitive the sulfur ligands are within these enzymes. Besides this, thiols such as cysteine play an important role in biological reduction/oxidation chemistry via disulfide formation, but also further oxidation to sulfenic, sulfinic, and sulfonic acids may occur.<sup>14–16</sup> Thus, gaining a better understanding of the oxidation of sulfur ligands in metallo-protein active sites is of interest. Herein we present a Cu<sup>I</sup> thiolate complex that is oxidized by dioxygen from air to form Cu<sup>II</sup> sulfinate and sulfonate complexes via a dinuclear Cu<sup>II</sup> thiolate intermediate, which bears similarity to the Cu<sub>A</sub> active site. Synthesis of the Cu<sup>I</sup> thiolate complex starting from the ligand Py<sub>2</sub>NSH [*N*-(2-mercaptopropyl)-*N,N*-bis(2-pyridylmethyl)amine] is depicted in Scheme 1. The Cu<sup>II</sup> sulfinate and Cu<sup>II</sup> sulfonate complexes have been isolated and studied by UV–vis and EPR spectroscopy as well as cyclic voltammetry.

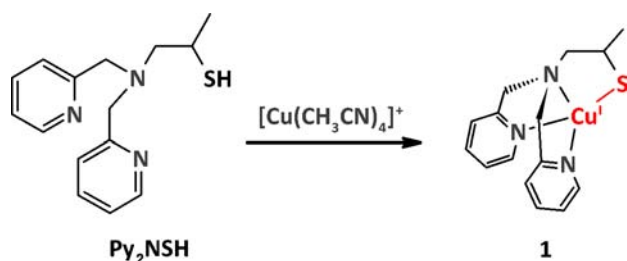
## EXPERIMENTAL SECTION

**Materials.** All chemicals were purchased from commercial sources and used as received. [Cu<sup>I</sup>(CH<sub>3</sub>CN)<sub>4</sub>](BF<sub>4</sub>), [Cu<sup>I</sup>(CH<sub>3</sub>CN)<sub>4</sub>](ClO<sub>4</sub>), and [Cu<sup>I</sup>(CH<sub>3</sub>CN)<sub>4</sub>](OTf) (HOTf = trifluoromethanesulfonic acid) were synthesized according to literature procedures.<sup>17,18</sup> All solvents were reagent grade. The synthesis of the ligand Py<sub>2</sub>NSH and the Cu<sup>I</sup> complexes were carried out using standard Schlenk-line techniques under an argon atmosphere. Solvents for these experiments were

Received: August 2, 2013

Published: October 30, 2013

**Scheme 1. Synthesis of Cu<sup>I</sup> Thiolate Compound (1) with Ligand Py<sub>2</sub>NSH**



distilled, deoxygenated by bubbling a stream of argon through the solution, and stored on activated molecular sieves under argon prior to use.

**Analytical Methods.** NMR spectra were recorded on a Bruker 300 DPX spectrometer. IR spectra were obtained on a Perkin-Elmer Paragon 1000 FTIR spectrophotometer equipped with a Golden Gate ATR device. X-band EPR derivative spectra were recorded with a Bruker EMXplus ESR spectrometer. Elemental analyses were performed using a Perkin-Elmer 2400 series II CHNS/O analyzer. Mass spectrometry was measured using a Finnigan Aqua mass spectrometer (MS) with electrospray ionization (ESI). Sample introduction was achieved through a Dionex ASI-100 automated sample injector with an eluent flow rate of 0.2 mL/min. HRMS spectra were recorded on a Thermo Finnigan LTQ Orbitrap equipped with an electrospray ion source in positive mode. UV-vis spectra were collected on a Perkin-Elmer Lambda 900 Spectrometer. In situ UV-vis spectra of the oxidation experiments were collected using a transmission dip probe with variable path length on an Avantes Avaspec-2048 spectrometer with Avalight-DH-S-BAL light source. Cyclic voltammetry was performed with an Autolab PGstat10 potentiostat controlled by GPES4 software. A three electrode arrangement with a glassy carbon working electrode (3 mm diameter), an Ag/AgCl double junction reference electrode, and a Pt wire counter electrode in acetone/0.1 M NBu<sub>4</sub>PF<sub>6</sub> was used. In these conditions the Fc/Fc<sup>+</sup> couple was found to be located at +525 mV, with a peak-to-peak separation of 62 mV. Potentials are given relative to the Ag/AgCl electrode.

**X-ray Structure Determinations.** [Cu<sup>II</sup><sub>4</sub>Cu<sup>I</sup><sub>4</sub>(Py<sub>2</sub>NS)<sub>4</sub>(μ-OH)<sub>2</sub>-(CH<sub>3</sub>CN)<sub>6</sub>](ClO<sub>4</sub>)<sub>6</sub>·2CH<sub>3</sub>CN (**2**) and [Cu<sup>II</sup><sub>2</sub>(Py<sub>2</sub>NSO<sub>2</sub>)<sub>2</sub>](OTf)<sub>2</sub> (**4b**). All reflection intensities for compounds **2** and **4b** were measured at 110(2) K using a KM4/Xcalibur diffractometer (detector: Sapphire3) with enhanced graphite-monochromated Mo Kα radiation (λ = 0.710 73 Å) under the program CrysAlisPro (Version 1.171.35.11 Oxford Diffraction Ltd., 2011). The program CrysAlisPro was used to refine the cell dimensions and for data reduction. The structures were solved with the program SHELXS-97<sup>19</sup> and were refined on F<sup>2</sup> with SHELXL-97.<sup>19</sup> Analytical numeric absorption corrections based on a multifaceted crystal model were applied using CrysAlisPro. The temperature of the data collection was controlled using the system Cryojet (manufactured by Oxford Instruments). The H atoms (unless otherwise specified) were placed at calculated positions using the instructions AFIX 13, AFIX 23, AFIX 43, or AFIX 137 with isotropic displacement parameters having values 1.2 or 1.5 times U<sub>eq</sub> of the attached C atoms.

[Cu<sup>II</sup><sub>2</sub>(Py<sub>2</sub>NSO<sub>2</sub>)<sub>2</sub>](BF<sub>4</sub>)<sub>2</sub>·2(CH<sub>3</sub>)<sub>2</sub>CO (**4a**). Reflections were measured on a Bruker Kappa Apex II diffractometer with sealed tube and Triumph monochromator (λ = 0.710 73 Å). The intensities were integrated with the program Eval15.<sup>20</sup> Absorption correction was performed with SADABS.<sup>21</sup> The structure was solved with direct methods using SHELXS-97.<sup>19</sup> Least-squares refinement was performed with SHELXL-2013<sup>19</sup> against F<sup>2</sup> of all reflections. Non-hydrogen atoms were refined freely with anisotropic displacement parameters. Hydrogen atoms were located in difference Fourier maps and refined with a riding model. Geometry calculations and checks for higher symmetry were performed with the PLATON program.<sup>22</sup>

**Ligand and Complex Synthesis.** *N*-(2-Mercaptopropyl)-*N,N*-bis(2-pyridylmethyl)amine (Py<sub>2</sub>NSH). Py<sub>2</sub>NSH was synthesized according to a reported procedure<sup>23</sup> with some modifications.

Di-(2-picolyl)amine (0.90 mL, 5.0 mmol) was dissolved in 10 mL of acetonitrile under argon. Propylene sulfide (0.59 mL, 7.5 mmol) was added, after which the reaction mixture was stirred for 15 h at 70 °C under argon. After the mixture had cooled down, the solvent and excess propylene sulfide were evaporated. The resulting yellow oil was purified by column chromatography (silica, eluent 4% methanol in dichloromethane) which yielded a light yellow oil (1.1 g, 4.0 mmol, 80%). <sup>1</sup>H NMR (300 MHz, CD<sub>3</sub>CN, RT): δ 1.21 (d, J = 7 Hz, 3H, C\*-CH<sub>3</sub>), 2.54 (dd, J = 13 Hz, 8 Hz, 1H, N-CH<sub>2</sub>-C\*), 2.66 (dd, J = 13 Hz, 6 Hz, 1H, N-CH<sub>2</sub>-C\*), 3.20 (m, 1H, C\*-H), 3.81 (dd, J = 29 Hz, 14 Hz, 4H, Py-CH<sub>2</sub>-N), 7.22 (m, 2H, Py-H<sub>5</sub>), 7.58 (d, J = 8 Hz, 2H, Py-H<sub>3</sub>), 7.73 (td, J = 8 Hz, 2 Hz, 2H, Py-H<sub>4</sub>), 8.52 (m, 2H, Py-H<sub>6</sub>). <sup>13</sup>C NMR (75 MHz, CD<sub>3</sub>CN, RT): δ 22.2 (C\*-CH<sub>3</sub>), 33.9 (C\*), 61.1 (Py-CH<sub>2</sub>-N), 64.3 (N-CH<sub>2</sub>-C\*), 122.9 (Py-C<sub>5</sub>), 124.1 (Py-C<sub>3</sub>), 137.1 (Py-C<sub>4</sub>), 149.7 (Py-C<sub>6</sub>), 160.3 (Py-C<sub>2</sub>). ESI-MS found (calcd) for [Py<sub>2</sub>NS-SNPpy<sub>2</sub> + H]<sup>+</sup> m/z 545.2 (545.3). IR (neat, cm<sup>-1</sup>): 2820w, 1589m, 1432m, 1148w, 1073w, 995w, 756s, 612w, 404m.

[Cu<sup>I</sup>(Py<sub>2</sub>NS)] (**1**). A 1 equiv portion of Py<sub>2</sub>NSH was mixed with 1 equiv of [Cu<sup>I</sup>(CH<sub>3</sub>CN)<sub>4</sub>](X) in either acetonitrile or acetone. This resulted in a light brown solution. For <sup>1</sup>H NMR, a solution of Py<sub>2</sub>NSH (0.24 mmol) and [Cu<sup>I</sup>(CH<sub>3</sub>CN)<sub>4</sub>](ClO<sub>4</sub>) (0.24 mmol) in 1.5 mL of deuterated acetonitrile was prepared under argon. NMR experiments were carried out under argon using a J. Young NMR tube. <sup>1</sup>H NMR (300 MHz, CD<sub>3</sub>CN, RT): δ 0.85 (br, 1H, C\*-CH<sub>3</sub>), 1.22 (br, 2H, C\*-CH<sub>3</sub>), 2.80 (br, 1H, N-CH<sub>2</sub>-C\*) 3.13 (br, 1H, N-CH<sub>2</sub>-C\*), 3.87 (br, 2H, C\*-H and Py-CH<sub>2</sub>-N), 4.33 (br, 3H, Py-CH<sub>2</sub>-N), 6.24 (br, 2H), 7.57 (br, 4H, Py-H), 8.05 (br, 2H, Py-H), 8.73 (br, 2H, Py-H). ESI-MS found (calcd) for [M]<sup>+</sup> m/z 335.0 (335.1); [M + O + H]<sup>+</sup> m/z 352.1 (352.0); [Py<sub>2</sub>NSSNPpy<sub>2</sub> + Cu]<sup>+</sup> m/z 607.3 (607.2); [2M]<sup>+</sup> m/z 670.3 (670.1).

Attempts to crystallize compound **1** by vapor diffusion of diethyl ether into an acetonitrile solution (X = ClO<sub>4</sub>) resulted in a brown oil with several types of crystals. X-ray crystallography of one of those crystals revealed the formation of a compound with formula [Cu<sup>II</sup><sub>4</sub>Cu<sup>I</sup><sub>4</sub>(Py<sub>2</sub>NS)<sub>4</sub>(μ-OH)<sub>2</sub>(CH<sub>3</sub>CN)<sub>6</sub>](ClO<sub>4</sub>)<sub>6</sub>·2CH<sub>3</sub>CN (**2**).

[Cu<sup>II</sup><sub>2</sub>(Py<sub>2</sub>NSO<sub>2</sub>)<sub>2</sub>](BF<sub>4</sub>)<sub>2</sub>·2(CH<sub>3</sub>)<sub>2</sub>CO (**4a**) and Cu<sup>II</sup><sub>2</sub>(Py<sub>2</sub>NSO<sub>2</sub>)<sub>2</sub>(BF<sub>4</sub>)<sub>2</sub> (**5a**). Py<sub>2</sub>NSH (32.5 mg, 0.12 mmol) was dissolved in 6 mL acetone under argon. The solution was further deoxygenated by bubbling argon through the solution. [Cu<sup>I</sup>(CH<sub>3</sub>CN)<sub>4</sub>](BF<sub>4</sub>) (38.4 mg, 0.12 mmol) was added, which resulted in a light brown solution. The solution was opened to the air and stirred for 2 h until the solution was green. The solution was diluted with 3 mL of acetone. Vials containing this reaction mixture were put into a larger container partially filled with diethyl ether, which was then tightly closed. Vapor diffusion of the diethyl ether into the reaction mixture resulted in bright green crystals of [Cu<sup>II</sup><sub>2</sub>(Py<sub>2</sub>NSO<sub>2</sub>)<sub>2</sub>](BF<sub>4</sub>)<sub>2</sub> (**4a**, 13 mg, 0.014 mmol, 24%), which were suitable for X-ray structure determination, together with a green powder of Cu<sup>II</sup><sub>2</sub>(Py<sub>2</sub>NSO<sub>2</sub>)<sub>2</sub>(BF<sub>4</sub>)<sub>2</sub> (**5a**, 19 mg, 0.020 mmol, 34%). The crystals of **4a** were handpicked from the mixture and dried for analysis.

Anal. Calcd for **4a**, C<sub>30</sub>H<sub>36</sub>B<sub>2</sub>Cu<sub>2</sub>F<sub>8</sub>N<sub>6</sub>O<sub>6</sub>S<sub>2</sub>: C 39.62, H 3.99, N 9.24, S 7.05. Found: C 39.46, H 4.04, N 9.18, S 7.00. ESI-MS found (calcd) for [1/2M - BF<sub>4</sub> - SO<sub>2</sub>]<sup>+</sup> m/z 302.9 (303.1); [1/2M - BF<sub>4</sub>]<sup>+</sup> m/z 367.9 (367.0); [1/2M - BF<sub>4</sub> + Na]<sup>+</sup> m/z 389.9 (390.0). HRMS found (calcd) for [1/2M - BF<sub>4</sub> - SO<sub>2</sub>]<sup>+</sup> m/z 303.08 (303.08); [1/2M - BF<sub>4</sub> - 2O]<sup>+</sup> m/z 335.07 (335.05); [1/2M - BF<sub>4</sub>]<sup>+</sup> m/z 367.04 (367.04); [1/2M + O - 2 H - BF<sub>4</sub>]<sup>+</sup> 381.07 (381.03); [M - 2 BF<sub>4</sub> + CF<sub>3</sub>COO]<sup>+</sup> m/z 849.07 (849.07). IR (neat, cm<sup>-1</sup>): 1606w, 1436w, 1046vs, 914s, 758m, 638w, 519w, 489w, 458w, 414w. UV-vis in acetonitrile at 0.1 mM [Cu] concentration: 262 nm (ε = 5800 M<sup>-1</sup> cm<sup>-1</sup>), 314 nm (ε = 900 M<sup>-1</sup> cm<sup>-1</sup>), 476 nm (ε = 450 M<sup>-1</sup> cm<sup>-1</sup>), 770 nm (ε = 120 M<sup>-1</sup> cm<sup>-1</sup>).

Anal. Calcd for **5a**, C<sub>30</sub>H<sub>36</sub>B<sub>2</sub>Cu<sub>2</sub>F<sub>8</sub>N<sub>6</sub>O<sub>6</sub>S<sub>2</sub>: C 38.27, H 3.85, N 8.93, S 6.81. Found: C 38.98, H 3.44, N 8.72, S 7.27. ESI-MS found (calcd) for [1/2M - BF<sub>4</sub> - SO<sub>3</sub>]<sup>+</sup> m/z 303.1 (303.1); [M - 2BF<sub>4</sub>]<sup>2+</sup> m/z 384.1 (384.0). IR (neat, cm<sup>-1</sup>): 1611w, 1448w, 1051vs, 1028vs, 767m, 656w, 521w, 423w. UV-vis in acetonitrile at 0.1 mM [Cu]

concentration: 262 nm ( $\epsilon = 9800 \text{ M}^{-1} \text{ cm}^{-1}$ ), 306 nm ( $\epsilon = 2200 \text{ M}^{-1} \text{ cm}^{-1}$ ), 490 nm ( $\epsilon = 250 \text{ M}^{-1} \text{ cm}^{-1}$ ), 740 nm ( $\epsilon = 90 \text{ M}^{-1} \text{ cm}^{-1}$ ).

$[\text{Cu}^{\text{II}}_2(\text{Py}_2\text{NSO}_2)_2(\text{OTf})_2]$  (**4b**) and  $\text{Cu}^{\text{II}}(\text{Py}_2\text{NSO}_3)_2(\text{OTf})_2$  (**5b**). Compounds **4b** and **5b** were synthesized in the same way as **4a** and **5a**, starting from  $\text{Py}_2\text{NSH}$  (60.8 mg, 0.22 mmol) and  $[\text{Cu}^{\text{I}}(\text{CH}_3\text{CN})_4](\text{OTf})$  (82.9 mg, 0.22 mmol). Diethyl ether diffusion yielded green crystals of  $[\text{Cu}^{\text{II}}_2(\text{Py}_2\text{NSO}_2)_2(\text{OTf})_2]$  (**4b**, 22 mg, 0.021 mmol, 21%) with green powder of  $\text{Cu}^{\text{II}}(\text{Py}_2\text{NSO}_3)_2(\text{OTf})_2$  (**5b**, 37 mg, 0.035 mmol, 31%).

Anal. Calcd for **4b**,  $\text{C}_{32}\text{H}_{36}\text{Cu}_2\text{F}_6\text{N}_6\text{O}_{10}\text{S}_4$ : C 37.17, H 3.51, N 8.13, S 12.40. Found: C 37.21, H 3.46, N 8.09, S 12.36. ESI-MS found (calcd) for  $[\frac{1}{2}\text{M} - \text{OTf} - \text{SO}_2]^+$   $m/z$  303.0 (303.1). IR (neat,  $\text{cm}^{-1}$ ): 1611w, 1448w, 1256s, 1142m, 1088s, 1030s, 852m, 766m, 632s, 573w, 516m, 420m.

Anal. Calcd for **5b**,  $\text{C}_{32}\text{H}_{36}\text{Cu}_2\text{F}_6\text{N}_6\text{O}_{12}\text{S}_4$ : C 36.05, H 3.40, N 7.88, S 12.03. Found: C 36.49, H 3.52, N 7.71, S 12.58. ESI-MS found (calcd)  $[\frac{1}{2}\text{M} - \text{OTf} - \text{SO}_3]^+$   $m/z$  303.0 (303.1);  $[\text{M} - 2\text{OTf}]^{2+}$   $m/z$  383.9 (384.0). HRMS found (calcd) for  $[\frac{1}{2}\text{M} - \text{OTf} - \text{SO}_3]^+$   $m/z$  303.08 (303.08);  $[\frac{1}{2}\text{M} - \text{BF}_4 - 3\text{O}]^+$   $m/z$  335.07 (335.05);  $[\frac{1}{2}\text{M} - \text{OTf} - \text{O}]^+$   $m/z$  367.04 (367.04);  $[\frac{1}{2}\text{M} - \text{OTf}]^+$   $m/z$  383.04 (383.04);  $[\frac{1}{2}\text{M} - \text{OTf} + \text{O}]^+$   $m/z$  399.01 (399.03);  $[(\text{Py}_2\text{NSO}_3) - (\text{Py}_2\text{NSO}_2) + \text{Na}]^+$   $m/z$  647.46 (647.21);  $[\text{Cu}(\text{Py}_2\text{NSO}_3)(\text{Py}_2\text{NSO}_2) + \text{OH} + 2 \text{Na}]^+$   $m/z$  750.41 (750.13). IR (neat,  $\text{cm}^{-1}$ ): 3441br, 1611w, 1448w, 1249s, 1155s, 1027vs, 767m, 636vs, 516m, 420w.

**UV Spectroscopic Monitoring of the Oxidation of  $[\text{Cu}(\text{Py}_2\text{NS})]$  (**1**).**  $\text{Py}_2\text{NSH}$  (5.5 mg, 0.02 mmol) was dissolved in acetone (2 mL) under argon.  $[\text{Cu}^{\text{I}}(\text{CH}_3\text{CN})_4](\text{BF}_4)$  (6.3 mg, 0.02 mmol) was added, which resulted in a light brown solution. The UV-vis setup with transmission dip probe (set at 1.2 mm path length) was put under argon and blanked with 8 mL of acetone, while stirring at 400 rpm. The solution of **1** was added to the UV-vis setup, giving a 2 mM  $[\text{Cu}]$  solution. Air was bubbled through the solution while measuring the absorbance spectrum for a period of 6 h.

## RESULTS

**Synthesis of Ligand and Complexes.** The ligand  $\text{Py}_2\text{NSH}$  was synthesized by reacting di-(2-picoly)amine with propylene sulfide as was previously reported.<sup>23</sup> Column chromatography was used to remove unreacted di-(2-picoly)amine. The thiol ligand  $\text{Py}_2\text{NSH}$  did not oxidize to the disulfide ligand  $\text{Py}_2\text{NS-SNPy}_2$  during the workup process, which was confirmed by chemically oxidizing  $\text{Py}_2\text{NSH}$  to  $\text{Py}_2\text{NS-SNPy}_2$  with iodine and comparison of the NMR spectra of the two compounds.<sup>24</sup> The ligand slowly degrades and cannot be kept for periods longer than a few months even when stored under argon at  $-20 \text{ }^\circ\text{C}$ . The ligand  $\text{Py}_2\text{NSH}$  is obtained as a mixture of the two enantiomers, as it possesses a chiral center. For all complexation experiments the racemic mixture was used. When either  $[\text{Cu}^{\text{I}}(\text{CH}_3\text{CN})_4](\text{BF}_4)$  or  $[\text{Cu}^{\text{I}}(\text{CH}_3\text{CN})_4](\text{OTf})$  was added to a solution of the ligand under argon, a highly oxygen-sensitive, light brown solution is obtained, which likely contains the complex  $\text{Cu}^{\text{I}}(\text{Py}_2\text{NS})$  (**1**, see Scheme 1). Although  $^1\text{H}$  NMR spectroscopy was measured under argon, the NMR spectrum only showed broad peaks in the diamagnetic region. The broadening of the NMR signals is most likely due to the presence of traces of  $\text{Cu}^{\text{II}}$ , or the presence of an equilibrium of different  $\text{Cu}^{\text{I}}$  species with partial coordination of the anions. However,  $^{19}\text{F}$  NMR spectra do not indicate coordination of the counterions to  $\text{Cu}^{\text{II}}$  species. ESI-MS of the light brown solution showed a peak pattern in agreement with  $[\text{Cu}(\text{Py}_2\text{NS})]^+$  and  $[\text{Cu}(\text{Py}_2\text{NSSNPy}_2)]^+$  (Supporting Information Figures S3–S9). Two smaller signals are also present: one that can tentatively be assigned to a mono-oxygenated compound  $[\text{Cu}(\text{Py}_2\text{NSO}) + \text{H}]^+$  or a hydroxide-containing compound  $[\text{Cu}(\text{Py}_2\text{NS}) + \text{OH}]^+$  and one signal that can be assigned to the dinuclear compound  $[\text{Cu}_2(\text{Py}_2\text{NS})_2]^+$ . Attempts to crystallize

complex **1** in acetonitrile (starting from the copper perchlorate salt) resulted in the formation of an oil with a number of different crystals. A crystal structure determination of one of those crystals showed the formation of the octanuclear, mixed-valent compound  $[\text{Cu}^{\text{II}}_4\text{Cu}^{\text{I}}_4(\text{Py}_2\text{NS})_4(\mu\text{-OH})_2(\text{CH}_3\text{CN})_6](\text{ClO}_4)_6 \cdot 2\text{CH}_3\text{CN}$  (**2**) (see below). The presence of  $\text{Cu}^{\text{II}}$  as well as  $\text{Cu}^{\text{I}}$  ions in this octanuclear cluster are in agreement with our explanation of the broad NMR signals observed for **1**. The origin of the  $\text{Cu}^{\text{II}}$  ions in this cluster is ascribed to partial oxidation by air, as no signs of disproportionation (metallic Cu) were observed. No other analyses of this compound could be obtained, due to its poor reproducibility. However, as we believe that the formation of this compound is typical for the reactivity of the copper system under study, we judged that it is worthwhile to discuss the structure of this cluster. Further oxidation of **1** (starting from the copper tetrafluoroborate (**a**) or triflate salt (**b**)) in air resulted in a color change from brown to dark green. After stirring for approximately 2 h at room temperature the solution had turned green. Slow diffusion of diethyl ether into the green solution resulted in green crystals, suitable for X-ray structure determination, and a green powder. The crystals and the powder were manually separated; X-ray diffraction showed that the crystals are dinuclear  $\text{Cu}^{\text{II}}$  sulfinate complexes  $[\text{Cu}^{\text{II}}_2(\text{Py}_2\text{NSO}_2)_2](\text{BF}_4)_2 \cdot 2(\text{CH}_3)_2\text{CO}$  (**4a**) and  $[\text{Cu}^{\text{II}}_2(\text{Py}_2\text{NSO}_2)_2(\text{OTf})_2]$  (**4b**), with different connectivity in the structures (see below), depending on the choice of the anion present in the starting  $\text{Cu}^{\text{I}}$  salt. ESI-MS spectra of complexes **4a** and **4b** both show a peak pattern that corresponds to one copper ion with one ligand without the  $\text{SO}_2$ -group (Supporting Information Figures S10–S14). Loss of an  $\text{SO}_2$  group upon fragmentation of sulfinate-containing ligands during ionization has been previously reported for nickel and palladium sulfinate complexes.<sup>25,26</sup> The spectrum of **4a** also shows two smaller signals that can be assigned to  $[\text{Cu}(\text{Py}_2\text{NSO}_2)]^+$  and  $[\text{Cu}(\text{Py}_2\text{NSO}_2) + \text{Na}]^+$ . The HRMS spectrum of **4a** shows a peak pattern for  $[\text{Cu}(\text{Py}_2\text{NSO}_2)]^+$  and  $[\text{Cu}_2(\text{Py}_2\text{NSO}_2)_2 + \text{F}_3\text{CCOO}]^+$  together with a range of other signals that indicate the instability of the  $\text{SO}_2$  group:  $[\text{Cu}(\text{Py}_2\text{NSO}_2) - \text{SO}_2]^+$ ,  $[\text{Cu}(\text{Py}_2\text{NS})]^+$ ,  $[\text{Cu}(\text{Py}_2\text{NSO}_3 - 2\text{H})]^+$  (Supporting Information Figures S15–S18). The powder EPR spectra of complexes **4a** and **4b** show an axial signal with  $g_{\parallel} = 2.18$  and  $g_{\perp} = 2.09$  (Supporting Information Figures S28–S29).

Analyses of the green powders indicate the formation of  $\text{Cu}^{\text{II}}$  sulfonate species. These complexes have been isolated with  $\text{BF}_4^-$  and  $\text{OTf}^-$  counterions, and are tentatively described as the dinuclear compounds  $\text{Cu}^{\text{II}}_2(\text{Py}_2\text{NSO}_3)_2(\text{BF}_4)_2$  (**5a**) and  $\text{Cu}^{\text{II}}_2(\text{Py}_2\text{NSO}_3)_2(\text{OTf})_2$  (**5b**). Unfortunately, all attempts to crystallize these  $\text{Cu}^{\text{II}}$  sulfonate species failed.  $\text{Cu}^{\text{II}}$  sulfonate complexes **5a** and **5b** have been analyzed with ESI-MS showing peak patterns corresponding to the dicationic complex  $[\text{Cu}_2(\text{Py}_2\text{NSO}_3)_2]^{2+}$  and the mononuclear complex with loss of the  $\text{SO}_3$  group (Supporting Information Figures S19–S21). The HRMS spectrum of complex **5b** shows a large number of signals resulting from reactivity of the  $\text{SO}_3$ -group similar to what was observed for the  $\text{SO}_2$ -group in **4a**:  $[\text{Cu}(\text{Py}_2\text{NSO}_3) - \text{SO}_3]^+$ ,  $[\text{Cu}(\text{Py}_2\text{NS})]^+$ ,  $[\text{Cu}(\text{Py}_2\text{NSO}_2)]^+$ ,  $[\text{Cu}(\text{Py}_2\text{NSO}_3) - (\text{Py}_2\text{NSO}_2) + \text{OH} + 2\text{Na}]^+$  (Supporting Information Figures S23–S27). A signal corresponding to a mononuclear species  $[\text{Cu}(\text{Py}_2\text{NSO}_3)]^+$  was also found in HRMS, in contrast to the ESI-MS spectrum in which a peak pattern for the dinuclear species  $[\text{Cu}_2(\text{Py}_2\text{NSO}_3)_2]^{2+}$  is present. Furthermore, a signal that may correspond to  $[\text{Cu}(\text{Py}_2\text{NOSO}_3)]^+$  is present, although

this signal can also be assigned to  $[\text{Cu}(\text{Py}_2\text{NSO}_2) + \text{CH}_3\text{OH}]^+$ . Powder EPR spectra of **5a** and **5b** both show an isotropic signal with  $g = 2.11$  (Supporting Information Figure S30).

**X-ray Crystallography. Description of Structure 2.** A projection of the structure of the cationic cluster of **2** is depicted in Figure 1, and crystallographic data are collected in

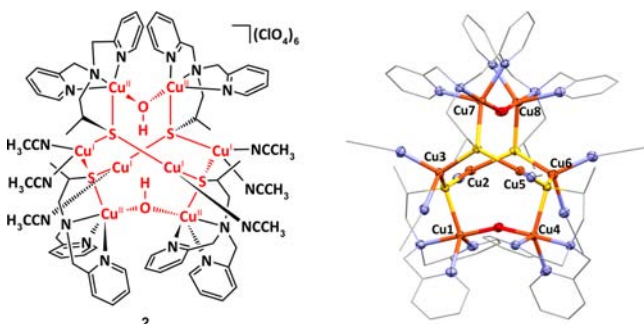


**Figure 1.** Schematic drawing and projection of the structure of the cationic part of  $[\text{Cu}^{\text{II}}_4\text{Cu}^{\text{I}}_4(\text{Py}_2\text{NS})_4(\mu\text{-OH})_2(\text{CH}_3\text{CN})_6](\text{ClO}_4)_6 \cdot 2\text{CH}_3\text{CN}$  (**2**). Displacement ellipsoids are depicted at the 50% probability level. All hydrogen atoms are omitted, and all carbon atoms are depicted in wireframe for clarity. Bond distance (Å) ranges:  $\text{Cu}^{\text{I}}\text{-S}$ , 2.22–2.31;  $\text{Cu}^{\text{II}}\text{-S}$ , 2.34–2.36;  $\text{Cu}^{\text{II}}\text{-O}$ , 1.91–1.94;  $\text{Cu}^{\text{I}}\text{-N}$ , 1.96–2.08;  $\text{Cu}^{\text{II}}\text{-N}$ , 2.03–2.05;  $\text{Cu}^{\text{II}}\text{-N}_{\text{py}}$ , 2.03–2.14.

Table 1. Selected bond angles and distances can be found in Supporting Information Table S1. The compound crystallizes in the centrosymmetric monoclinic space group  $C2/c$ , with one complex cluster, six perchlorate ions, and two molecules of acetonitrile per asymmetric unit. The crystal structure is mostly ordered except for three of the six perchlorate counterions, which are found to be disordered over two or three orientations. Complex **2** is an octanuclear mixed-valent copper species with the formula  $[\text{Cu}^{\text{II}}_4\text{Cu}^{\text{I}}_4(\text{Py}_2\text{NS})_4(\mu\text{-}$

$\text{OH})_2(\text{CH}_3\text{CN})_6](\text{ClO}_4)_6$ . The cluster contains four  $\text{Cu}^{\text{I}}$  and four  $\text{Cu}^{\text{II}}$  ions with two hydroxide and four  $\text{Py}_2\text{NS}^-$  ligands.

The structure can be described as two dinuclear  $\{\text{Cu}^{\text{II}}_2(\text{Py}_2\text{NS})_2(\text{OH})\}$  units in which the copper ions are singly bridged by the hydroxide group; these dinuclear units are held together by four  $\text{Cu}^{\text{I}}$  ions. Each  $\text{Cu}^{\text{I}}$  ion is bridging between two different thiolate groups from two ligands (one from each dinuclear unit) and is bound to either one or two acetonitrile ligands. The central bridging structure thus comprises two  $\text{Cu}^{\text{I}}$  ions with trigonal  $\text{NS}_2$  coordination and two  $\text{Cu}^{\text{I}}$  ions with tetrahedral  $\text{N}_2\text{S}_2$  coordination. The  $\text{Cu}^{\text{II}}$  ions are in an  $\text{N}_3\text{OS}$  environment, in a geometry that is best described as a highly distorted trigonal bipyramid with the hydroxide oxygen and amine nitrogen at the axial positions and  $\tau$  values ranging between 0.63 and 0.82.<sup>27</sup> Contrary to what is expected, the  $\text{Cu}\text{-S}$  distances of the smaller  $\text{Cu}^{\text{II}}$  ion are larger than the  $\text{Cu}\text{-S}$  distances for  $\text{Cu}^{\text{I}}$ . The longer  $\text{Cu}^{\text{II}}\text{-S}$  distances might be caused by the presence of the hydroxide ion bridging the two  $\text{Cu}^{\text{II}}$  ions. The hydroxyl hydrogen is positioned between the two thiolate sulfurs forming a bifurcated  $\text{O}\text{-H}\cdots\text{S}$  hydrogen bond, with  $\text{H}\cdots\text{S}$  distances of 2.75–2.85 Å. An analogous pentanuclear  $\text{Fe}^{\text{II}}$  complex has been reported,<sup>28</sup> which contains a ligand very similar to  $\text{Py}_2\text{NS}$ . The structure is built up of similar  $\{\text{Fe}^{\text{II}}_2(\text{N}_3\text{S})_2(\text{OH})\}$  units, but instead of being held together by four metal ions, one  $\text{Fe}^{\text{II}}$  ion holds these fragments together, and the bridging hydroxide group is pointing away from the thiolate sulfurs.

**Description of Structures 4a and 4b.** The crystal structures of two dinuclear  $\text{Cu}^{\text{II}}$  sulfinate complexes with either  $\text{BF}_4^-$  counterions  $[\text{Cu}^{\text{II}}_2(\text{Py}_2\text{NSO}_2)_2](\text{BF}_4)_2 \cdot 2(\text{CH}_3)_2\text{CO}$  (**4a**) or  $\text{OTf}^-$  counterions  $[\text{Cu}^{\text{II}}_2(\text{Py}_2\text{NSO}_2)_2(\text{OTf})_2]$  (**4b**) were determined. Projections of the cationic dinuclear structure of **4a** and the structure of **4b** are depicted in Figure 2; crystallographic data and selected bond distances and angles are given in Tables 1 and 2, respectively.

**Table 1. Crystallographic and Structure Refinement Data for Complexes 2, 4a, and 4b**

	2	4a	4b
empirical formula	$[\text{C}_{72}\text{H}_{92}\text{Cu}_8\text{N}_{18}\text{O}_2\text{S}_4](\text{ClO}_4)_6 \cdot 2\text{C}_2\text{H}_5\text{N}$	$[\text{C}_{30}\text{H}_{36}\text{Cu}_2\text{N}_6\text{O}_4\text{S}_2](\text{BF}_4)_2 \cdot 2\text{C}_3\text{H}_6\text{O}$	$\text{C}_{32}\text{H}_{36}\text{Cu}_2\text{F}_6\text{N}_6\text{O}_{10}\text{S}_4$
fw	2557.00	1025.62	1033.99
cryst syst	monoclinic	monoclinic	monoclinic
space group	$C2/c$	$C2/c$	$P2_1/c$
$a$ , Å	27.0514(3)	29.4214(15)	9.3137(3)
$b$ , Å	38.7599(3)	9.2998(4)	12.4946(4)
$c$ , Å	23.0026(3)	21.3070(7)	16.8065(5)
$\beta$ , deg	113.4265(15)	130.288(2)	100.346(3)
$V$ , Å <sup>3</sup>	22130.4(4)	4447.0(3)	1923.99(10)
$Z$	8	4	2
$D_{\text{calc}}$ , g cm <sup>-3</sup>	1.535	1.532	1.785
$T$ , K	110(2)	150(2)	110(2)
cryst size, mm <sup>3</sup>	$0.40 \times 0.26 \times 0.13$	$0.50 \times 0.30 \times 0.23$	$0.38 \times 0.20 \times 0.13$
$\mu$ , mm <sup>-1</sup>	1.801	1.134	1.417
no. reflns measured	80 859	35 196	13 441
no. unique reflns	19 488	5082	3378
no. reflns obsd	15 932 [ $I > 2\sigma(I)$ ]	4465 [ $I > 2\sigma(I)$ ]	2833 [ $I > 2\sigma(I)$ ]
no. params	1434	283	345
$R1/wR2$ [ $I > 2\sigma(I)$ ]	0.0335/0.0889	0.0275/0.0692	0.0546/0.1516
$R1/wR2$ (all reflns)	0.0438/0.0928	0.0338/0.0724	0.0668/0.1605
GOF	1.076	1.084	1.069
$\Delta\rho$ , e Å <sup>-3</sup>	-0.59/0.87	-0.47/0.64	-0.55/1.11

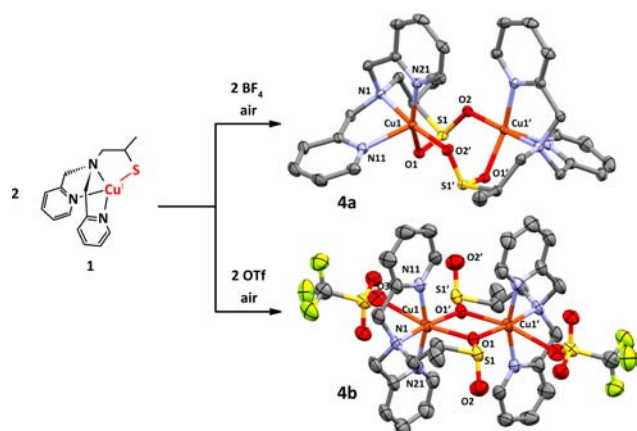


**Figure 2.** Schematic overview of the oxidation of  $\text{Cu}^{\text{I}}(\text{Py}_2\text{NS})$  (**1**) to  $[\text{Cu}^{\text{II}}_2(\text{Py}_2\text{NSO}_2)_2](\text{BF}_4)_2 \cdot 2(\text{CH}_3)_2\text{CO}$  (**4a**) and  $[\text{Cu}^{\text{II}}_2(\text{Py}_2\text{NSO}_2)_2(\text{OTf})_2]$  (**4b**). The projections of the crystal structures of complex **4b** and the cationic part of **4a** are depicted. Displacement ellipsoids are shown at the 50% probability level. All hydrogen atoms are omitted for clarity.

Compound **4a** crystallizes in the monoclinic space group  $C2/c$ , with half a dinuclear compound, one molecule of acetone, and one  $\text{BF}_4^-$  ion in the asymmetric unit; the dinuclear compound is located on a 2-fold rotation axis. Compound **4b** crystallizes in the monoclinic space group  $P2_1/c$ , with one crystallographically independent half of the dinuclear compound in the asymmetric unit (i.e., the dinuclear copper complex is found at sites of inversion symmetry). In complex **4a** the two symmetry-related  $\text{Cu}^{\text{II}}$  ions are bridged by the two  $\text{SO}_2^-$  groups, forming an eight-membered ring consisting of  $\text{Cu1}$ ,  $\text{O1}$ ,  $\text{S1}$ ,  $\text{O2}$ ,  $\text{Cu1}'$ ,  $\text{O1}'$ ,  $\text{S1}'$ ,  $\text{O2}'$  (Figure 2). This configuration is associated with a lower degree of strain than that of the four-membered ring  $\text{Cu}(\mu\text{-O})_2\text{Cu}$  found in **4b**; the coordination angle  $\text{O1}-\text{Cu1}-\text{O2}'$  is  $93.72(5)^\circ$  in **4a**, whereas the bond angle  $\text{O1}-\text{Cu1}-\text{O1}'$  is  $75.56(13)^\circ$  in **4b**. The copper

ions in **4a** are in an  $\text{N}_3\text{O}_2$  coordination environment with distorted square-pyramidal geometry ( $\tau = 0.28^{27}$ ).

The di(pyridylmethyl)amine group is bound in a facial manner, with the pyridyl groups located in *cis* positions relative to each other. One of the pyridyl groups is located at the axial position at a distance of  $2.1706(15)$  Å; the basal plane is formed by the other pyridyl nitrogen, the amine nitrogen, and the two sulfonate oxygens. The S–O distances within the  $\text{SO}_2^-$  group are more or less equal ( $1.5247(13)$  and  $1.5377(13)$  Å), indicating full delocalization of the electrons. Although the  $\text{Cu}^{\text{II}}$  centers are bridged by a three-atom structure, the Cu–Cu distance is relatively short at  $3.6322(5)$  Å because of a weakly chelating interaction of the second sulfonate oxygen: The Cu1–O2 distance is  $2.8833(16)$  Å, which can be considered as semicoordinating. With this interaction taken into account, the coordination geometry of the copper center can be regarded as elongated octahedral with the pyridyl N11 and O2 located on the Jahn–Teller axis. The  $\text{BF}_4^-$  anion is not coordinated.

The  $\text{Cu}^{\text{II}}$  centers in **4b** are also symmetry related and are doubly bridged by two oxygens, one of each of the sulfonate groups, resulting in a planar  $\text{Cu}(\mu\text{-O})_2\text{Cu}$  arrangement. The  $\text{OTf}^-$  counterions are coordinated to the copper centers resulting in an  $\text{N}_3\text{O}_3$  environment. The  $\text{OTf}^-$  counterions are disordered over two orientations with relative occupancies of  $0.638(5)$  and  $0.362(5)$ . The  $\text{Cu}^{\text{II}}$  ions are in a Jahn–Teller elongated octahedral geometry with the triflate O3 and sulfonate O1 atoms in the axial positions at  $2.600(8)$  and  $2.415(3)$  Å, respectively. The di-(2-pyridylmethyl)amine group is bound in a meridional fashion in the equatorial plane, with the pyridyl groups in *trans* position relative to each other; the fourth position of the equatorial plane is occupied by the sulfonate oxygen O1' of the symmetry-related molecule. In contrast with compound **4a**, the S–O distances within the  $\text{SO}_2^-$  group in **4b** are dissimilar. The S1–O1 distance is  $1.56$  Å, and the S1–O2 distance is  $1.46$  Å. This indicates that the S1–O1 bond has more of a single-bond character while the S1–O2 bond has more of a double bond character; the atom O1 with single-bond characteristics is coordinated to the Cu ions.

**Table 2.** Selected Bond Distances and Angles of **4a** and **4b**

	bond distance (Å)		bond angle (deg)	
	<b>4a</b>	<b>4b</b>	<b>4a</b>	<b>4b</b>
Cu1–Cu1' <sup>a</sup>	3.6322(3)	3.4679(7)	O1–Cu1–O2'	93.72(5)
Cu1–O1	1.9956(12)	2.415(3)	O1–Cu1–O1'	75.56(13)
Cu1–O1'		1.959(3)	O2–Cu1–O2'	84.52(6)
Cu1–O2	2.8833(16)		O1–Cu1–N1	87.06(5)
Cu1–O2'	1.9698(12)		O1–Cu1–N11	93.89(5)
Cu1–O3		2.600(8)	O1–Cu1–N21	155.46(6)
Cu1–S1	2.9271(7)		N1–Cu1–N11	80.67(6)
Cu1–S1'	3.0825(6)	3.1152(13)	N1–Cu1–N21	84.43(6)
Cu1–N1	2.0417(14)	2.025(4)	N1–Cu1–O1	94.47(14)
Cu1–N11	2.1706(15)	1.990(4)	N1–Cu1–O2	172.25(7)
Cu1–N21	1.9877(15)	2.016(4)	N11–Cu1–N21	107.32(6)
S1–O1	1.5247(13)	1.555(3)	N11–Cu1–O1	160.83(16)
S1–O2	1.5377(13)	1.461(4)	N11–Cu1–O2	94.43(14)
			N21–Cu1–O1	100.39(14)
			N21–Cu1–O2	91.78(7)
			O1–S1–O2	107.88(7)
			Cu1–O1–Cu1	104.44(13)
			Cu1–O2–Cu1'	95.05(7)

<sup>a</sup> =  $1 - x, y, 1/2 - z$  for **4a** and  $-x, 1/2 + y, 1/2 - z$  for **4b**.

Similar S–O distances have been reported for other Cu<sup>II</sup> sulfinate complexes.<sup>29,30</sup> The Cu–Cu distance of 3.468 Å is slightly smaller than that in **4a**. The Py<sub>2</sub>NSO<sub>2</sub><sup>−</sup> enantiomers form *RR* and *SS* complexes in the crystal structure of **4a**, but are evenly distributed with one *R*-isomer and one *S*-isomer per dinuclear complex in the crystal structure of **4b**.

**Solution Studies.** Solutions of the sulfinato–Cu<sup>II</sup> complexes **4a** and **4b** in acetonitrile give the same UV–vis spectra (Supporting Information Figure S35), showing a  $\pi^* \leftarrow \pi$  transition of the pyridyl groups at 262 nm, an LMCT of Cu<sup>II</sup>  $\leftarrow$  O at 314 nm, and two transitions at 476 and 770 nm. The transition at 770 nm can be ascribed to a d–d transition of the copper(II) ion. The high  $\epsilon$  value ( $\epsilon = 450 \text{ M}^{-1} \text{ cm}^{-1}$ ) of the transition at 476 nm indicates that this absorption must be ascribed to a second Cu<sup>II</sup>  $\leftarrow$  O LMCT. The similarity of the spectra indicates that the OTf<sup>−</sup> counterion of **4b** does not remain coordinated in solution. When UV spectra of the complexes are recorded at higher concentrations, the absorbance at 476 nm disappears, while a new band arises at 370 nm (see Figure 3). This behavior may indicate that in solution the dinuclear Cu<sup>II</sup> complex is in equilibrium with its monomeric form depending on the concentration.

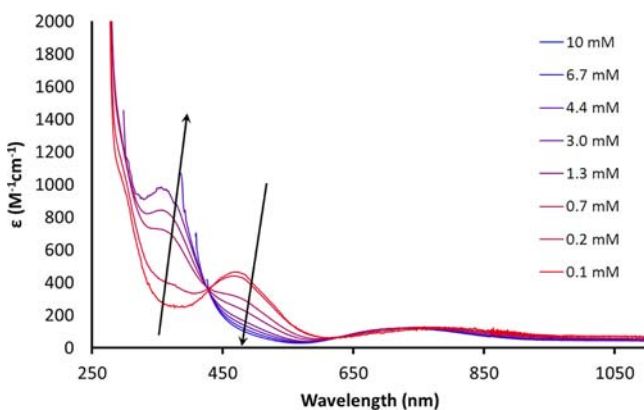


**Figure 3.** UV–vis spectra of  $[\text{Cu}^{\text{II}}_2(\text{Py}_2\text{NSO}_2)_2](\text{BF}_4)_2 \cdot 2(\text{CH}_3)_2\text{CO}$  (**4a**) at different concentrations ranging from 0.1 to 10 mM [Cu] in acetonitrile. The arrows show the development of the spectra upon increasing complex concentration.

The sulfinato–Cu<sup>II</sup> complexes **5a** and **5b** also show the same UV–vis spectra in acetonitrile solution, indicating that also in these compounds the counterions do not coordinate to the copper centers in solution (Supporting Information Figure S36). The absorbance spectra of **5a** and **5b** show bands similar to those of **4a** and **4b**, with the  $\pi^* \leftarrow \pi$  transition of the pyridyl groups at 262 nm, oxygen to copper LMCT at 306 and 490 nm, and a d–d transition 740 nm. The effect of the complex concentration on the absorbance, as observed for complex **4a**, is also present for **5a**, but the changes are much smaller (Supporting Information Figure S37). With increasing complex concentration, the absorbance at 490 nm decreases, and a small increase in absorbance takes place at 378 nm.

The sulfinate compounds **4a** and **4b** show highly similar solution EPR spectra in both acetone and acetonitrile solutions at room temperature. The spectra predominantly show a mononuclear isotropic signal at  $g_{\text{I}} = 2.11$  with a copper hyperfine splitting of 63 G (Figure 4). In addition to the signal of the mononuclear species, a weak axial triplet signal is observed, with a half field signal at 1600 G, indicating the presence of two ferromagnetically interacting Cu<sup>II</sup> ions

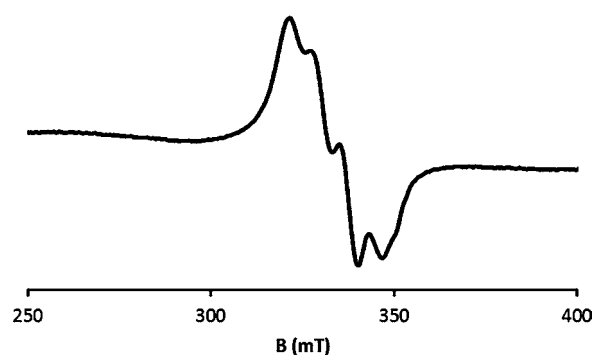


**Figure 4.** X-band EPR spectrum at RT of  $[\text{Cu}^{\text{II}}_2(\text{Py}_2\text{NSO}_2)_2](\text{OTf})_2$  (**4b**) dissolved in acetonitrile ( $\nu = 9.874 \text{ GHz}$ ).

(Supporting Information Figure S31).<sup>31,32</sup> The isotropic signal of **4b** was simulated (Supporting Information Figure S32) showing the copper hyperfine coupling to be 185 MHz. EPR solution spectra of the sulfonate compounds **5a** and **5b** are very similar to the spectra of **4a** and **4b** (Supporting Information Figures S33–S34), showing similar weak axial triplet spectra overlaid with isotropic signals. A weak half-field signal was observed for **5a** and **5b** in acetone, but this signal was not visible in acetonitrile.

Cyclic voltammograms of **4a** were recorded in acetone solutions. The voltammogram shows two quasireversible waves (Figure 5a). The first wave is located at  $E_{1/2} = -306 \text{ mV}$  with a peak to peak separation of 121 mV; the second electrochemical event is centered at  $E_{1/2} = -74 \text{ mV}$  with a peak to peak separation of 182 mV. When the concentration of the compound was increased from 1 mM [Cu] to 2 mM [Cu] the ratio of the peak currents of the two events ( $\Delta I_1/\Delta I_2$ ) slightly changed from 1.0 to 1.1, indicating that the two redox events may be ascribed to the presence of a mononuclear and a dinuclear species as observed in the UV–vis spectra; the redox event at  $-306 \text{ mV}$  may thus possibly be attributed to the dinuclear species.

The cyclic voltammogram of Cu<sup>II</sup> sulfonate compound **5a** is different from that of compound **4a** and shows no reversible electrochemical events (Figure 5b). At least three reduction events ( $E_{\text{pc}}$  at  $-103$ ,  $-345$ , and  $-939 \text{ mV}$ ) and three oxidation waves ( $E_{\text{pa}}$  at  $-345$ ,  $310$ , and  $783 \text{ mV}$ ) are observed. The CV of complex **5a** is reproducible when the electrode is polished in between measurements. When this is not done small shifts in the peak potentials are observed. The reduction wave at  $-939 \text{ mV}$  shifts to more positive potentials at higher scan rates and more negative potentials at lower scan rates (Supporting Information Figure S39).

**UV–Vis Monitoring of the Oxidation of 1.** The oxidation of Cu<sup>I</sup>(Py<sub>2</sub>NS) (**1**) to the sulfinate and sulfonate species was monitored using UV–vis spectroscopy. When a solution of **1** is opened to air, a new species starts to form as indicated by a color change from light brown to dark green (Figure 6a). The solution was kept homogeneous by bubbling air through the solution and stirring at 400 rpm. An absorbance band at 372 nm arises within three minutes, which is likely to be a thiolate to Cu<sup>II</sup> LMCT. Two bands at 573 and 910 nm of lower intensity appear which may be attributed to d–d transitions. A UV–vis spectrum recorded for a freshly prepared solution containing  $[\text{Cu}^{\text{I}}(\text{H}_2\text{O})_6](\text{BF}_4)_2$  and Py<sub>2</sub>NSH shows the same characteristic bands at 372, 573, and 910 nm (Supporting Information Figure S38). When this solution is left

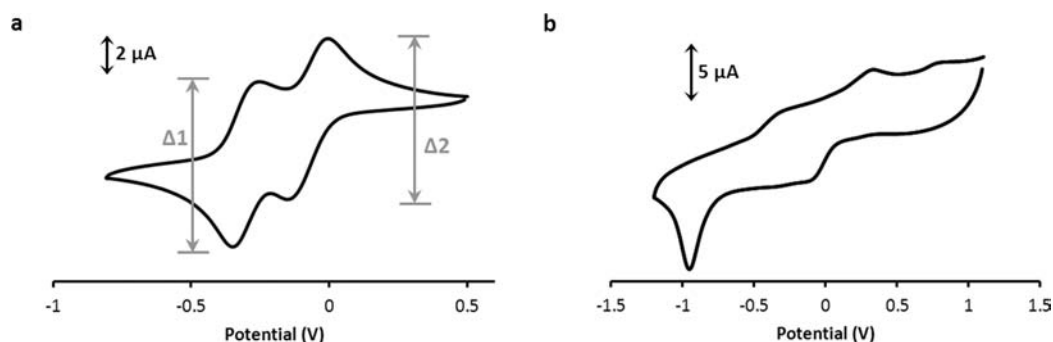


**Figure 5.** Cyclic voltammogram of (a)  $[\text{Cu}^{\text{II}}_2(\text{Py}_2\text{NSO}_2)_2](\text{BF}_4)_2 \cdot 2(\text{CH}_3)_2\text{CO}$  (**4a**) and (b)  $\text{Cu}^{\text{II}}_2(\text{Py}_2\text{NSO}_3)_2(\text{BF}_4)_2$  (**5a**) in acetone at 1 mM  $[\text{Cu}]$  concentration at RT. The scan rate is 100 mV/s; potentials are given vs Ag/AgCl.

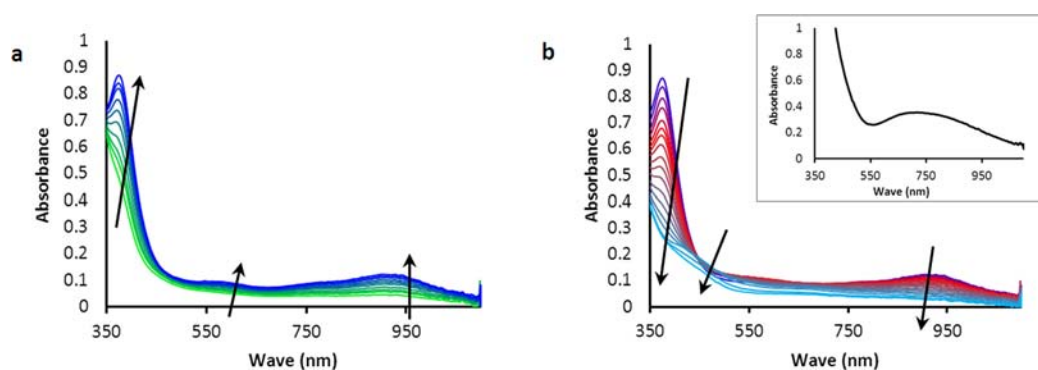


**Figure 6.** UV-vis spectral changes observed for an acetone solution of  $[\text{Cu}^{\text{I}}(\text{Py}_2\text{NS})](\text{BF}_4)$  (**1**) with concentration of 2 mM  $[\text{Cu}]$  exposed to air for 6 h. (a) Appearance of absorbance bands in first three minutes and (b) decrease of absorbance bands over 6 h; inset shows UV-vis spectrum of the fully oxidized complex **1** at 6.0 mM  $[\text{Cu}]$  recorded with a transmission dip probe path length of 3.4 mm.

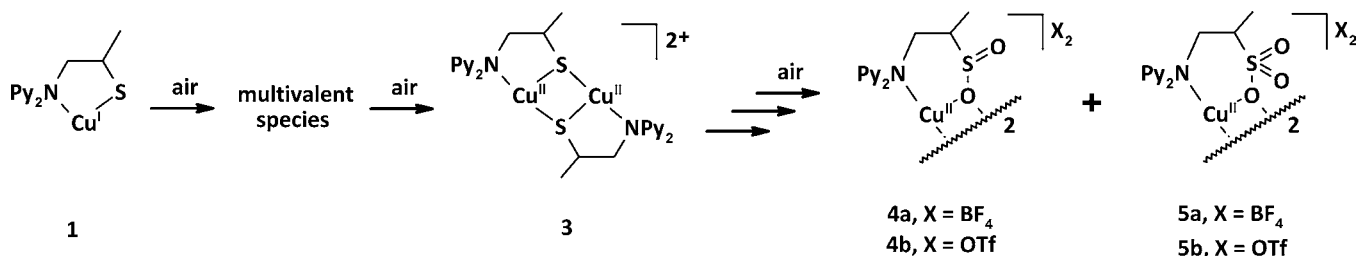


**Figure 7.** Schematic overview of the complete oxidation of  $\text{Cu}^{\text{I}}(\text{Py}_2\text{NS})$  (**1**).  $\text{Py}_2\text{N}$  = di-2-(picolyamine).

in air for a period of 6 h, the solution slowly turns lighter green; the characteristic bands for the intermediate species disappear, indicating further oxidation of the copper compound (Figure 6b). In the spectrum of the fully oxidized species a broad d-d transition is observed (inset in Figure 6b) in agreement with the presence of both the sulfinate (**4**, 770 nm) and sulfonate (**5**, 740 nm) species.

## DISCUSSION

When  $\text{Py}_2\text{NSH}$  is reacted with  $[\text{Cu}^{\text{I}}(\text{CH}_3\text{CN})_4](\text{BF}_4)$  in acetone, a species is formed that is tentatively formulated as  $\text{Cu}^{\text{I}}(\text{Py}_2\text{NS})$  (**1**), although the formation of dinuclear or oligonuclear species cannot be ruled out. Compound **1** is highly oxidation sensitive, as suggested by the broad NMR signals that are indicative for the presence of traces of  $\text{Cu}^{\text{II}}$ . When species **1** is brought into contact with air,  $\text{Cu}^{\text{I}}$  is oxidized to  $\text{Cu}^{\text{II}}$  before the thiolate ligand is oxidized. In an attempt to crystallize the  $\text{Cu}^{\text{I}}$  thiolate complex, the multivalent compound **2** was isolated, which may be regarded as an intermediate in the oxidation process; in this compound  $\text{Cu}^{\text{II}}$  as well as  $\text{Cu}^{\text{I}}$  centers are

present, whereas the thiolate ligands are not yet oxidized. In the initial stage of the oxidation process, the formation of a species with specific absorption bands at 372, 573, and 910 nm is indicative for the oxidation of  $\text{Cu}^{\text{I}}$  to  $\text{Cu}^{\text{II}}$ , generating a species that can be formulated as  $[\text{Cu}^{\text{II}}_2(\text{Py}_2\text{NS})_2]^{2+}$  (**3**) (see below). The UV-vis spectrum generated upon partial oxidation of the  $\text{Cu}^{\text{I}}$  thiolate solution with air is the same as the spectrum that is obtained when a  $\text{Cu}^{\text{II}}$  salt is reacted with  $\text{Py}_2\text{NSH}$  in an otherwise oxygen-free solution (Supporting Information Figure S38). When  $\text{Cu}^{\text{II}}$  thiolate species **3** is further oxidized by dioxygen,  $\text{Cu}^{\text{II}}$  sulfinate (**4a**, **4b**) and  $\text{Cu}^{\text{II}}$  sulfonate (**5a**, **5b**) complexes are obtained. A complete overview of the observed reactivity of  $\text{Cu}^{\text{I}}(\text{Py}_2\text{NS})$  (**1**) in air is given in Figure 7.

Although  $\text{Cu}^{\text{II}}$  thiolate compounds are relatively rare due to the high reactivity that usually results in the immediate formation of  $\text{Cu}^{\text{I}}$  and disulfide,<sup>33</sup> structures of a number of  $\text{Cu}^{\text{II}}$  thiolate species have been reported. Notably, the group of Itoh reported the structures of two dinuclear  $\text{Cu}^{\text{II}}$  thiolate coordination compounds of ligands that are highly similar to the one we used in our study.<sup>34,35</sup> Schematic structures of these

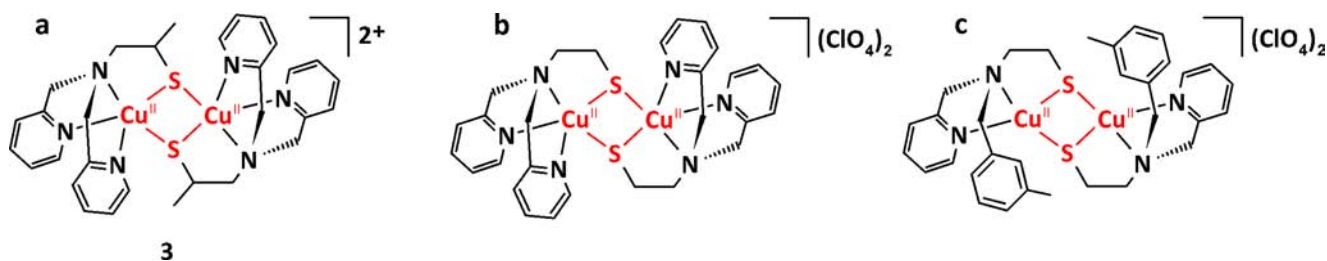


**Figure 8.** Schematic drawings of dinuclear  $\text{Cu}^{\text{II}}$   $\mu$ -thiolate complexes. (a) Proposed structure for compound 3. Structures reported by Itoh et al. (b) from ref 35 and (c) from ref 34.

compounds together with the postulated structure of compound 3 are given in Figure 8. The di- $\mu$ -thiolato  $\text{Cu}^{\text{II}}$  complex shown in Figure 8b shows absorbance bands in the UV-vis spectrum at 366, 556, and 884 nm.<sup>35</sup> These bands are comparable to those observed for 3, corroborating our proposal for its dinuclear structure.

The  $\text{Cu}_2\text{S}_2$  core in the dinuclear species 3 bears some resemblance to the  $\text{Cu}_A$  site; the oxidation of 3 into  $\text{Cu}^{\text{II}}$  sulfinate and  $\text{Cu}^{\text{II}}$  sulfonate species may thus provide information about possible deactivation pathways of the  $\text{Cu}_A$  active site and possibly other copper-sulfur enzymes such as  $\beta\text{M}$ .

Quite some research has been carried out on models for dioxygen-induced degradation of enzymes. Most investigations have been focused on nickel,<sup>26,36–38</sup> but also the oxygenation reactions of thiolate complexes of other metals such as cobalt,<sup>39,40</sup> iron,<sup>41–43</sup> and zinc<sup>44</sup> have been studied. Some studies on the oxidation of copper-sulfur compounds have been reported, but the chemistry is greatly complicated by the ability of copper to catalyze disulfide formation and cleavage.<sup>33,35</sup> A  $\text{Cu}^{\text{I}}$  compound has been reported to form a  $\text{Cu}^{\text{II}}$  sulfonate complex starting from either a disulfide or a thiolate ligand.<sup>45</sup> Similarly, the generation of a  $\text{Cu}^{\text{II}}$  sulfinate compound starting from  $\text{Cu}^{\text{II}}$  with a disulfide ligand<sup>29</sup> or a sulfonate-containing complex starting from a thiolate ligand has been reported.<sup>46</sup> Noteworthy is also the formation of  $\text{Cu}^{\text{I}}$  disulfide and  $\text{Cu}^{\text{II}}$  sulfinate species from a  $\text{Cu}^{\text{II}}$  disulfide complex under anaerobic conditions in water.<sup>30</sup> The mechanisms behind these reactions are very complicated and seem to differ depending on the ligand. It appears that the ligand largely determines the coordination environment of the copper center and whether a  $\text{Cu}^{\text{I}}$  disulfide species or a  $\text{Cu}^{\text{II}}$  thiolate species is formed as the most stable configuration.<sup>35</sup> The oxidation reaction of these two species most likely will follow different mechanisms. The dipyriddy-thiolate ligand  $\text{Py}_2\text{NSH}$  used in our studies generates a dinuclear  $\text{Cu}^{\text{II}}$   $\mu$ -thiolate instead of a  $\text{Cu}^{\text{I}}$  disulfide compound upon reaction with a  $\text{Cu}^{\text{II}}$  salt. This corroborates our finding that the oxidation of  $\text{Cu}^{\text{I}}(\text{Py}_2\text{NS})$  proceeds via the oxidation of  $\text{Cu}^{\text{I}}$  to  $\text{Cu}^{\text{II}}$  before the oxygenation of the ligand takes place.

The exact mechanism of oxygenation of the thiolate ligand is not yet clear. The ESI-MS of complex 1 shows a small signal that may tentatively be ascribed to either a copper-sulfenate or a copper-hydroxide species, either of which could be intermediates in the oxidation reaction. All attempts at isolation of other intermediates in addition to compound 2 failed. To the best of our knowledge, there are no previous reports in which both a  $\text{Cu}^{\text{II}}$  sulfinate and a  $\text{Cu}^{\text{II}}$  sulfonate complex were isolated and characterized. This gives us the unique opportunity to compare the properties of both types of complexes.

The UV-vis spectra of the sulfinate and the sulfonate complexes show many similarities. Both spectra show oxygen to  $\text{Cu}^{\text{II}}$  LMCT and two d-d transitions at roughly the same wavelengths. The EPR and UV-vis spectra of the two sulfinate complexes 4a and 4b dissolved in either acetone or acetonitrile are highly comparable, indicating that the counterion dissociates and the same  $[\text{Cu}^{\text{II}}_2(\text{Py}_2\text{NSO}_2)_2]^{2+}$  species is present in solution. The changes observed in these spectra, depending on the concentration of the copper compounds, indicate the presence of both monomeric and dimeric species in an equilibrium reaction. The same behavior is observed for the sulfonate complexes 5a and 5b, indicating that these are most likely also dinuclear in the solid state with general formula  $[\text{Cu}^{\text{II}}_2(\text{Py}_2\text{NSO}_3)_2]^{2+}$ . For the  $\text{Cu}^{\text{II}}$  sulfonate complexes the equilibrium in solution seems to be more directed toward the dinuclear species; the increase of the band at 490 nm for the  $\text{Cu}^{\text{II}}$  sulfonate compound with dilution is much smaller than the increase at 476 nm for the  $\text{Cu}^{\text{II}}$  sulfinate complex. Furthermore, for the  $\text{Cu}^{\text{II}}$  sulfonate compounds a signal in the ESI-MS can be ascribed to the dicationic, dinuclear species. The solution EPR spectra of the  $\text{Cu}^{\text{II}}$  sulfinate and  $\text{Cu}^{\text{II}}$  sulfonate compounds are also very similar, both showing the presence of the monomeric as well as dimeric species in solution.

Whereas the spectroscopic data for the  $\text{Cu}^{\text{II}}$  sulfinate and  $\text{Cu}^{\text{II}}$  sulfonate complexes are very similar, the electrochemical properties on the other hand are dissimilar. The cyclic voltammogram of  $\text{Cu}^{\text{II}}$  sulfinate complex 4a shows two quasireversible waves. These two waves may tentatively be ascribed again to the presence of monomeric and dimeric species, in which case the  $\text{Cu}^{\text{II}}$  to  $\text{Cu}^{\text{I}}$  reduction would take place at different potentials for each species. Alternatively, since the ratio of peak currents shows only a small change upon a small concentration difference, the two waves can be assigned to two separate one-electron reductions of the dinuclear compound, with a stable  $\text{Cu}^{\text{II}}\text{Cu}^{\text{I}}$  intermediate.<sup>47</sup> However, for dinuclear systems similar to 4a also single isolated two-electron events have been reported.<sup>47</sup> With the available data it is not possible to decide which assignment is appropriate. In contrast, the cyclic voltammogram of  $\text{Cu}^{\text{II}}$  sulfonate compound 5a shows several irreversible events. A possible explanation for the irreversibility could be the difference in hardness of the sulfonate group as compared to the sulfinate group; the softer sulfinate group is more likely to stabilize the  $\text{Cu}^{\text{I}}$  oxidation state as it can also bind with the sulfur atom. To be able to compare  $\text{Cu}^{\text{II}}$  sulfinate and  $\text{Cu}^{\text{II}}$  sulfonate complexes in more detail, a crystal structure of the sulfonate compound would be helpful. Furthermore, it would be very interesting to isolate other intermediates such as a  $\text{Cu}^{\text{II}}$  sulfenate complex, because until now such a compound has not been reported.



## CONCLUSION

Cu<sup>II</sup> sulfinate and Cu<sup>II</sup> sulfonate complexes, that were formed by the oxidation of a Cu<sup>I</sup> thiolate species, were isolated and analyzed. Elucidation of the mechanism for oxygenation of the thiolate ligands in the Cu<sup>II</sup> thiolate species toward the Cu<sup>II</sup> sulfinate and Cu<sup>II</sup> sulfonate complexes could give information about the degradation pathways of copper–sulfur enzymes by dioxygen. UV–vis spectroscopy shows that oxidation of the Cu<sup>I</sup> thiolate complex is very likely to proceed via the formation of a dinuclear Cu<sup>II</sup> thiolate compound that bears resemblance to the Cu<sub>A</sub> active site. The oxidation of Cu<sup>I</sup> to Cu<sup>II</sup> takes place before the thiolate ligand is oxygenated, which could be caused by the tendency of this type of complex to form Cu<sup>II</sup> thiolate species rather than Cu<sup>I</sup> disulfide species. Spectroscopic and electrochemical analysis of the Cu<sup>II</sup> sulfinate and Cu<sup>II</sup> sulfonate complexes showed that both species are spectroscopically very similar, but electrochemically very different. This difference in electrochemical properties is most likely caused by the relative hardness of the sulfonate group that is not suitable for stabilization of the Cu<sup>I</sup> oxidation state.

## ASSOCIATED CONTENT

### Supporting Information

Crystallographic data of **2** (CIF format) including bond distances and angles and difference Fourier maps of the H-atoms, all ESI-MS and HRMS spectra, EPR spectra, UV–vis spectra, and the cyclic voltammogram of **5a** at different scan rates. This material is available free of charge via the Internet at <http://pubs.acs.org>.

## AUTHOR INFORMATION

### Corresponding Author

\*E-mail: [bouwman@chem.leidenuniv.nl](mailto:bouwman@chem.leidenuniv.nl)

### Notes

The authors declare no competing financial interest.

## ACKNOWLEDGMENTS

This research has been financially supported by the National Graduate Research School Combination NRSC-Catalysis, a joint activity of the graduate research schools NIOK, HRSMC, and PTN. We thank John van Dijk for ESI-MS analysis, Hans van den Elst for HRMS measurements, and Jos van Brussel for elemental analysis. We also thank Fons Lefeber and Karthick Sai Sankar Gupta for assistance with NMR and Prof. Dr. Bas de Bruin (University of Amsterdam) for his help with EPR simulations.

## REFERENCES

- (1) Belle, C.; Rammal, W.; Pierre, J. L. *J. Inorg. Biochem.* **2005**, *99*, 1929–1936.
- (2) Yoshizawa, K.; Kihara, N.; Kamachi, T.; Shiota, Y. *Inorg. Chem.* **2006**, *45*, 3034–3041.
- (3) Prigge, S. T.; Kolhekar, A. S.; Eipper, B. A.; Mains, R. E.; Amzel, L. M. *Science* **1997**, *278*, 1300–1305.
- (4) Prigge, S. T.; Kolhekar, A. S.; Eipper, B. A.; Mains, R. E.; Amzel, L. M. *Nat. Struct. Biol.* **1999**, *6*, 976–983.
- (5) Prigge, S. T.; Eipper, B. A.; Mains, R. E.; Amzel, L. M. *Science* **2004**, *304*, 864–867.
- (6) Klinman, J. P. *Chem. Rev.* **1996**, *96*, 2541–2561.
- (7) Solomon, E. I.; Penfield, K. W.; Gewirth, A. A.; Lowery, M. D.; Shadle, S. E.; Guckert, J. A.; LaCroix, L. B. *Inorg. Chim. Acta* **1996**, *243*, 67–78.

- (8) Guckert, J. A.; Lowery, M. D.; Solomon, E. I. *J. Am. Chem. Soc.* **1995**, *117*, 2817–2844.
- (9) Larsson, S.; Broo, A.; Sjölin, L. *J. Phys. Chem.* **1995**, *99*, 4860–4865.
- (10) Iwata, S.; Ostermeier, C.; Ludwig, B.; Michel, H. *Nature* **1995**, *376*, 660–669.
- (11) Tsukihara, T.; Aoyama, H.; Yamashita, E.; Tomizaki, T.; Yamaguchi, H.; Shinzawaitoh, K.; Nakashima, R.; Yaono, R.; Yoshikawa, S. *Science* **1995**, *269*, 1069–1074.
- (12) Wilmanns, M.; Lappalainen, P.; Kelly, M.; SauerEriksson, E.; Saraste, M. *Proc. Natl. Acad. Sci. U.S.A.* **1995**, *92*, 11955–11959.
- (13) Brown, K.; Tegoni, M.; Prudencio, M.; Pereira, A. S.; Besson, S.; Moura, J. J.; Moura, I.; Cambillau, C. *Nat. Struct. Biol.* **2000**, *7*, 191–195.
- (14) Jacob, C.; Giles, G. L.; Giles, N. M.; Sies, H. *Angew. Chem., Int. Ed.* **2003**, *42*, 4742–4758.
- (15) Katayama, Y.; Hashimoto, K.; Nakayama, H.; Mino, H.; Nojiri, M.; Ono, T.; Nyunoya, H.; Yohda, M.; Takio, K.; Odaka, M. *J. Am. Chem. Soc.* **2006**, *128*, 728–729.
- (16) Shigehiro, S.; Nakasako, M.; Dohmae, N.; Tsujimura, M.; Tokoi, K.; Odaka, M.; Yohda, M.; Kamiya, N.; Endo, I. *Nat. Struct. Biol.* **1998**, *5*, 347–351.
- (17) Irangu, J.; Ferguson, M. J.; Jordan, R. B. *Inorg. Chem.* **2005**, *44*, 1619–1625.
- (18) Pennings, Y. C. M.; Driessen, W. L.; Reedijk, J. *Polyhedron* **1988**, *7*, 2583–2589.
- (19) Sheldrick, G. M. *Acta Crystallogr., Sect. A* **2008**, *64*, 112–122.
- (20) Schreurs, A. M. M.; Xian, X.; Kroon-Batenburg, L. M. J. *J. Appl. Crystallogr.* **2010**, *43*, 70–82.
- (21) Sheldrick, G. M. *SADABS: Area-Detector Absorption Correction*; Universität Göttingen: Göttingen, Germany, 1999.
- (22) Spek, A. L. *Acta Crystallogr., Sect. D* **2009**, *65*, 148–155.
- (23) Angamuthu, R.; Byers, P.; Lutz, M.; Spek, A. L.; Bouwman, E. *Science* **2010**, *327*, 313–315.
- (24) <sup>1</sup>H NMR of Py<sub>2</sub>NS-SNPpy<sub>2</sub> (300 MHz, CD<sub>3</sub>CN, RT): δ 1.16 (dd, J = 6 Hz, 1 Hz, 6H, C\*–CH<sub>3</sub>), 2.55 (dd, J = 13 Hz, 8 Hz, 2H, N–CH<sub>2</sub>–C\*), 2.70 (m, 2H, N–CH<sub>2</sub>–C\*), 3.01 (m, 2H, C\*–H), 3.73 (s, 4H, Py–CH<sub>2</sub>–N), 3.74 (s, 4H, Py–CH<sub>2</sub>–N), 7.14 (m, 4H, Py–H<sub>3</sub>), 7.52 (d, J = 8 Hz, 4H, Py–H<sub>3</sub>), 7.65 (td, J = 8 Hz, 2 Hz, 4H, Py–H<sub>4</sub>), 8.44 (m, 2H, Py–H<sub>6</sub>).
- (25) Tuntulani, T.; Musie, G.; Reibenspies, J. H.; Darensbourg, M. Y. *Inorg. Chem.* **1995**, *34*, 6279–6286.
- (26) Buonomo, R. M.; Font, I.; Maguire, M. J.; Reibenspies, J. H.; Tuntulani, T.; Darensbourg, M. Y. *J. Am. Chem. Soc.* **1995**, *117*, 963–973.
- (27) Addison, A. W.; Rao, T. N.; Reedijk, J.; Vanrijn, J.; Verschoor, G. C. *J. Chem. Soc., Dalton Trans.* **1984**, 1349–1356.
- (28) Krishnamurthy, D.; Sarjeant, A. N.; Goldberg, D. P.; Caneschi, A.; Totti, F.; Zakharov, L. N.; Rheingold, A. L. *Chem.—Eur. J.* **2005**, *11*, 7328–7341.
- (29) Odani, A.; Maruyama, T.; Yamauchi, O.; Fujiwara, T.; Tomita, K. *J. Chem. Soc., Chem. Commun.* **1982**, 646–647.
- (30) Higashi, L. S.; Lundeen, M.; Hilti, E.; Seff, K. *Inorg. Chem.* **1977**, *16*, 310–313.
- (31) Koolhaas, G. J. A. A.; Driessen, W. L.; Reedijk, J.; van der Plas, J. L.; de Graaff, R. A. G.; Gatteschi, D.; Kooijman, H.; Spek, A. L. *Inorg. Chem.* **1996**, *35*, 1509–1517.
- (32) Mabbs, F. E.; Collison, D. *Electron Paramagnetic Resonance of d Transition Metal Compounds*; Elsevier: Amsterdam, 1992.
- (33) Ohta, T.; Tachiyama, T.; Yoshizawa, K.; Yamabe, T. *Tetrahedron Lett.* **2000**, *41*, 2581–2585.
- (34) Ueno, Y.; Tachi, Y.; Itoh, S. *J. Am. Chem. Soc.* **2002**, *124*, 12428–12429.
- (35) Itoh, S.; Nagagawa, M.; Fukuzumi, S. *J. Am. Chem. Soc.* **2001**, *123*, 4087–4088.
- (36) Mirza, S. A.; Pressler, M. A.; Kumar, M.; Day, R. O.; Maroney, M. J. *Inorg. Chem.* **1993**, *32*, 977–987.
- (37) Henderson, R. K.; Bouwman, E.; Spek, A. L.; Reedijk, J. *Inorg. Chem.* **1997**, *36*, 4616–4617.

- (38) Hosler, E. R.; Herbst, R. W.; Maroney, M. J.; Chohan, B. S. *Dalton Trans.* **2012**, *41*, 804–816.
- (39) Bourles, E.; de Sousa, R. A.; Galardon, E.; Giorgi, M.; Artaud, I. *Angew. Chem., Int. Ed.* **2005**, *44*, 6162–6165.
- (40) Adzamlı, I. K.; Libson, K.; Lydon, J. D.; Elder, R. C.; Deutsch, E. *Inorg. Chem.* **1979**, *18*, 303–311.
- (41) Lugo-Mas, P.; Dey, A.; Xu, L.; Davin, S. D.; Benedict, J.; Kaminsky, W.; Hodgson, K. O.; Hedman, B.; Solomon, E. I.; Kovacs, J. *A. J. Am. Chem. Soc.* **2006**, *128*, 11211–11221.
- (42) Sallmann, M.; Siewert, I.; Fohlmeister, L.; Limberg, C.; Knispel, C. *Angew. Chem., Int. Ed.* **2012**, *51*, 2234–2237.
- (43) McQuilken, A. C.; Goldberg, D. P. *Dalton Trans.* **2012**, *41*, 10883–10899.
- (44) de Sousa, R. A.; Galardon, E.; Rat, M.; Giorgi, M.; Artaud, I. *J. Inorg. Biochem.* **2005**, *99*, 690–697.
- (45) Lee, Y.; Lee, D.-H.; Sarjeant, A. A. N.; Karlin, K. D. *J. Inorg. Biochem.* **2007**, *101*, 1845–1858.
- (46) Stange, A.; Schurr, T.; Klein, A.; Kaim, W. Z. *Anorg. Allg. Chem.* **2005**, *631*, 663–671.
- (47) Zanello, P.; Tamburini, S.; Vigato, P. A.; Mazzocchin, G. A. *Coord. Chem. Rev.* **1987**, *77*, 165–273.